THREE-DIMENSIONAL VARIATIONAL ANALYSIS OF IMPACT CONTACT DEFORMATION OF THICK COMPOSITE PLATES

A. E. Bogdanovich and S. P. Yushanov

3TEX, Inc., 1017 Main Campus Drive, Suite 3200, Raleigh, NC 27606, U.S.A.

SUMMARY: Three-dimensional variational dynamic contact analysis approach is developed for predicting deformation of composite plates exposed to a rigid body impact. The Hamilton variational principle is applied using Bernstein basis functions of an arbitrary degree for the displacement approximation in all coordinate directions. Lagrange multiplier technique is employed in formulation of the variational dynamic contact problem. Input of the analysis uses only mass, velocity and nose shape of the projectile, without any assumed contact law. One specific application of the approach is illustrated on the example of thick bi-material composite rectangular bar exposed to a longitudinal rigid body impact. Numerical results illustrate time variations of the longitudinal displacement and strain, impact contact pressure, total energy of the system, and the total energy components. It is shown that, at a given incipient impact energy, the relative contribution of each energy component is highly dependent on the projectile mass and velocity.

KEYWORDS: impact, composite plates, variational analysis, 3-D elasticity, contact problems.

INTRODUCTION

In several papers and reference books [1-8] one can find thorough reviews of numerous analysis approaches and numerical results for the problems of impact deformation and failure of composite plates. Among those, the approach first reported in [9] and then further elaborated in [6] has its distinct place, as noted in review paper [7]. The following features of that approach are important in the context of present work: (I) each layer in a laminated structure is treated as 3-D orthotropic elastic solid with the continuity of displacements enforced between the layers; (II) a non-penetration condition between the composite plate and rigid projectile is enforced using Lagrange multiplier technique; (III) impact contact zone between the plate and projectile has variable size, which is one of the unknowns (a specially developed numerical iteration procedure was used to evaluate it). Accordingly, the approach does not assume *a priori* any

impact contact law (the projectile effect is fully characterized by its nose shape, mass and initial velocity). If required, the contact law can be assessed *a posteriori*, from the solution results. In the other words, the time- and coordinate-dependent surface pressure acting on the target, as well as the time-dependent size of the contact area are direct outputs of the analysis. Also, this approach allows one to analyze stress wave propagation processes in the through-thickness and in-plane directions of a laminated composite target. However, the algorithms developed in [6] are only applicable to the two-dimensional (cylindrical bending) problems of rectangular plates.

Presents work inherits certain features of the approach [6], but extends the methodology to a full 3-D case. This novel variational impact contact analysis approach uses Bernstein basis functions in all three coordinate directions, instead of B-splines applied in [9] and [6]. A detailed presentation of this new mathematical development can be found in [10]. Due to this, present paper provides only brief synopsis of the approach. Numerical example illustrates application of this approach to the problem of longitudinal impact on thick rectangular bi-material (metal-composite) bar. A comparison between numerical results obtained with the present 3-D contact analysis and 3-D dynamic non-contact analysis [11] (in the latter one the impact loading history was evaluated from the energy and momentum conservation laws) is discussed.

3-D VARIATIONAL IMPACT CONTACT ANALYSIS OF COMPOSITE PLATES

Consider 3-D problem of impact deformation of a rectangular plate composed from solid bricks, as illustrated in Fig. 1. Generally, each brick (treated as generally anisotropic elastic solid with all 21 independent elastic constants accounted in the analysis) may have its distinct elastic properties. This feature allows applying this approach not only to traditional cross-ply and angle-ply laminates and sandwiches, but also to various types of 3D textiles (woven, braided, knitted, etc.). In a particular case of laminated plates, all bricks belonging to the same layer have identical properties, while a step-wise property variation takes place at the interfaces perpendicular to the *z*-axis.

The build-up of a generic 3-D mosaic composite body shown in Fig. 2 is fully defined by three sets of orthogonal planes: $x = x_l$, $y = y_m$, and $z = z_n$ ($l = 2,...,L$, $m = 2,...,M$, $n = 2,...,N$). Thus, there are LMN bricks in the body. The discretization planes, which separate distinct material bricks, are true interfaces while those discretization planes which separate bricks made from the same material have purely computational meaning. Numbers of the planes in three coordinate directions have only computational limitations. One distinctive feature of this analysis approach is that it enables to impose different internal boundary conditions between any two adjacent bricks for the cases of (i) bricks made from different materials, (ii) bricks made from the same material, and (iii) surface crack between the bricks.
The stress-strain relations for the sth brick are written as

$$\sigma_i^{(s)}(\mathbf{r},t) = C_{ij}^{(s)}\varepsilon_j^{(s)}(\mathbf{r},t), \quad i, j = 1,...,6 \tag{1}$$

where $\sigma_i^{(s)}$ and $\varepsilon_j^{(s)}$ are stresses and strains, $C_{ij}^{(s)}$ are stiffness matrix components, $\mathbf{r} = \{x, y, z\}$ is a position vector, and t is time variable. In the present version of the analysis, the above strains are related to the displacements $u_1(x,y,z,t)$, $u_2(x,y,z,t)$ and $u_3(x,y,z,t)$ in the x, y and z directions through conventional equations of linear 3-D elasticity.

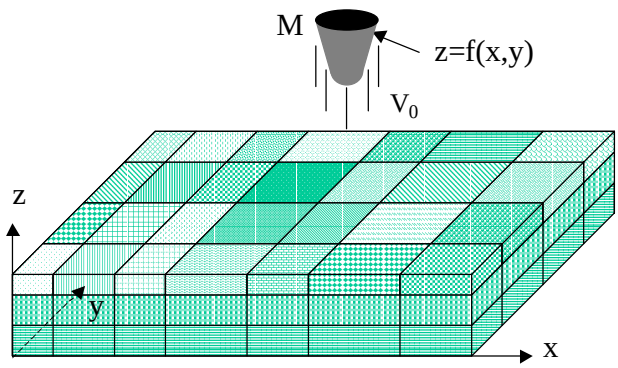

Fig. 1: Transverse impact on a composite plate

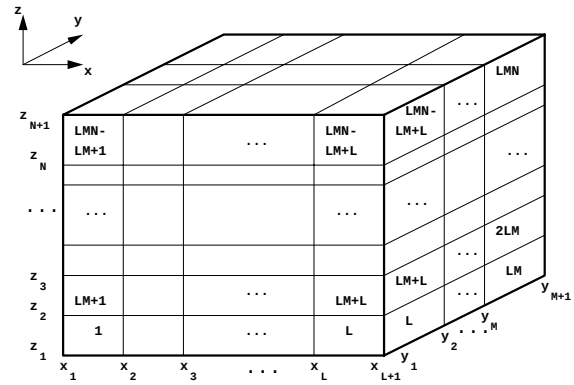

Fig. 2: Generic 3-D Mosaic Model of a composite solid

Three-dimensional variational analysis of mechanical system “mosaic composite body-rigid projectile” is based on the Hamilton variational principle

$$\delta \int_{t_1}^{t_2} L(t)dt = 0 \tag{2}$$

where *L(t)* is the Lagrange function of the whole system containing kinetic energy of the projectile $K_P(t)$, kinetic energy of the target $K_T(t)$, potential energy of the target $\Pi_T(t)$ (this incorporates strain energy $P_T(t)$ and work of external surface forces $W_T(t)$), and the "contact interaction" energy term $V_{PT}(t)$:

$$L(t) = K_P(t) + K_T(t) - \Pi_T(t) + V_{PT}(t) = K_P(t) + \sum_{s=1}^{S}\left[K_T^{(s)}(t) - P_T^{(s)}(t) + W_T^{(s)}(t)\right] + V_{PT}(t) \tag{3}$$

Here, $K_T^{(s)}$, $P_T^{(s)}$ and $W_T^{(s)}$ are kinetic energy, strain energy and work of external surface forces of the sth brick, respectively. In order to obtain their explicit expressions, some specific form of the displacement approximation is to be taken. Here we assume that the displacement field in the sth brick may be represented in the following form:

$$u_\alpha^{(s)}(x,y,z,t) = \sum_{i=0}^{I}\sum_{j=0}^{J}\sum_{k=0}^{K} U_{ijk}^{\alpha(s)}(t) X_i(x) Y_j(y) Z_k(z)\,; \quad \alpha = 1,2,3 \tag{4}$$

where the integers *I*, *J* and *K* define primary number of degrees of freedom (d.o.f.) contained in the primary computational model (this number is reduced after applying internal and external kinematic boundary conditions); $U_{ijk}^{\alpha(s)}(t)$ are undetermined time functions; $X_i(x)$, $Y_j(y)$ and $Z_k(z)$ are three sets of basis functions which have to be specified in each particular mathematical algorithm. In the present analysis, following [10], Bernstein basis functions are applied in the three coordinate directions. Specifically the following basis functions are taken for the parallelepiped located between the planes x_l and x_{l+1}, y_m and y_{m+1}, z_n and z_{n+1}:

$$X_i(x) = \begin{cases} B_i^I(x) = \dfrac{I!}{i!(I-i)!}\left(\dfrac{x - x_l}{x_{l+1} - x_l}\right)^i \left(\dfrac{x_{l+1} - x}{x_{l+1} - x_l}\right)^{I-i} & for\ \ x \in [x_l, x_{l+1}] \\ 0 \quad else \end{cases} \tag{5}$$

$$Y_j(y) = \begin{cases} B_j^J(y) = \dfrac{J!}{j!(J-j)!}\left(\dfrac{y-y_m}{y_{m+1}-y_m}\right)^j\left(\dfrac{y_{m+1}-y}{y_{m+1}-y_m}\right)^{J-j} & for\ \ y \in [y_m, y_{m+1}] \\ 0 \quad else \end{cases} \tag{6}$$

$$Z_k(z) = \begin{cases} B_k^K(z) = \dfrac{K!}{k!(K-k)!}\left(\dfrac{z-z_n}{z_{n+1}-z_n}\right)^k\left(\dfrac{z_{n+1}-z}{z_{n+1}-z_n}\right)^{K-k} & for\ \ z \in [z_n, z_{n+1}] \\ 0 \quad else \end{cases} \tag{7}$$

The triad of integers *l*, *m* and *n* defines location of all boundaries between the bricks. The above Bernstein basis functions possess certain unique properties that make them extremely suitable for developing elegant mathematical solutions and computational algorithms for various boundary value problems of solid mechanics. First, as shown in [10], the integrals involved in definitions of the stiffness and mass matrices, can be derived as closed-form analytical expressions, so avoiding approximate Gauss-type procedures. Second, as shown in [10], basis functions defined by Eqs 5-7 enable to express the displacement continuity conditions between the bricks in a 3-D mosaic body as the following simple relations:

$$U_{Ijk}^{\alpha,s(l,m,n)}(t) = U_{0jk}^{\alpha,s(l+1,m,n)}(t) \tag{8}$$

$$U_{iJk}^{\alpha,s(l,m,n)}(t) = U_{i0k}^{\alpha,s(l,m+1,n)}(t) \tag{9}$$

$$U_{ijK}^{\alpha,s(l,m,n)}(t) = U_{ij0}^{\alpha,s(l,m,n+1)}(t) \tag{10}$$

which should be satisfied for the corresponding values of *s*, *i*, *j* and *k*. If all of the Eqs 8-10 are satisfied, then the solution of any specific boundary value problem automatically provides continuous displacement field *everywhere* within mosaic body shown in Fig. 2. Also, as shown in [10], continuity of transverse stresses can be imposed between any two adjacent bricks made from the same material, in addition to the displacement continuity conditions. The corresponding relations between undetermined coefficients $U_{ijk}^{\alpha(s)}(t)$ .have been derived in [10]. Besides, as shown in [10] Bernstein basis functions are allowing to *identically* satisfy external kinematic boundary conditions in the case of *uniformly* distributed displacements (imposed either at some part or along the whole exterior surface of the mosaic body). Another property, which seems beneficial from the standpoint of stress/strain convergence, is that the Bernstein polynomials yield so-called *smooth approximants* e.g., they provide simultaneous approximation not only for the function, but also for its *derivatives* (see [12] for more detail).

Further, using Eqs 4-7, analytical expressions of $P_T^{(s)}$, $W_T^{(s)}$ and $K_T^{(s)}$ entering in Eqn 3 can be derived. The result is written in the form

$$P_T^{(s)}(t) = \frac{1}{2}\sum_{i=0}^{I}\sum_{j=0}^{J}\sum_{k=0}^{K}\sum_{p=0}^{I}\sum_{q=0}^{J}\sum_{r=0}^{K}\sum_{\alpha=1}^{3}\sum_{\beta=1}^{3} U_{ijk}^{\beta(s)}(t) a_{ijk,pqr}^{\alpha\beta(s)} U_{pqr}^{\alpha(s)}(t) = \frac{1}{2}\mathbf{U}^{(s)T}(t)\mathbf{A}^{(s)}\mathbf{U}^{(s)}(t) \tag{11}$$

$$W_T^{(s)}(t) = \sum_{i=0}^{I}\sum_{j=0}^{J}\sum_{k=0}^{K}\sum_{\alpha=1}^{3} U_{ijk}^{\alpha(s)}(t) Q_{ijk}^{\alpha(s)}(t) = \mathbf{U}^{(s)T}(t)\mathbf{Q}^{(s)}(t) \tag{12}$$

$$K_T^{(s)}(t) = \frac{1}{2}\sum_{i=0}^{I}\sum_{j=0}^{J}\sum_{k=0}^{K}\sum_{p=0}^{I}\sum_{q=0}^{J}\sum_{r=0}^{K}\sum_{\alpha=1}^{3} m_{ijk,pqr}^{\alpha\alpha(s)} \frac{dU_{ijk}^{\alpha(s)}(t)}{dt}\frac{dU_{pqr}^{\alpha(s)}(t)}{dt} = \frac{1}{2}\dot{\mathbf{U}}^{(s)T}(t)\mathbf{M}^{(s)}\dot{\mathbf{U}}^{(s)}(t) \tag{13}$$

Here, $\mathbf{U}^{(s)}(t)$ is the vector of undetermined displacement coefficients, $\mathbf{A}^{(s)}$ is the stiffness matrix, and $\mathbf{Q}^{(s)}(t)$ is the vector of external surface tractions; their explicit expressions can be found in [10]. Further, nonzero elements of the mass matrix $\mathbf{M}^{(s)}$ are

$$m_{ijk,pqr}^{11(s)} = m_{ijk,pqr}^{22(s)} = m_{ijk,pqr}^{33(s)} = \rho^{(s)} X_{ip} Y_{jq} Z_{kr} \tag{14}$$

where

$$X_{ip} = \int_{x_l}^{x_{l+1}} X_i(x) X_p(x) dx\,,\; Y_{jq} = \int_{y_m}^{y_{m+1}} Y_j(y) Y_q(y) dy\,,\; Z_{kr} = \int_{z_n}^{z_{n+1}} Z_k(z) Z_r(z) dz \tag{15}$$

Kinetic energy of the projectile is defined through its mass M and displacement as a rigid body $U(t)$:

$$K_I(t) = \frac{1}{2} M \left(\frac{dU}{dt} \right)^2 \tag{16}$$

After that, all what remains is to derive expression of the interactive term $V_{IT}(t)$ by considering contact interaction between the plate and rigid projectile.

The impact contact model adopted in this work assumes that upper surface of the plate is exposed to the contact pressure, which is undetermined function of the coordinates x and y and time t. A significant algorithmic assumption used here is that dimensions of the contact area in the x and y directions change incrementally during the time integration procedure. This means that during each specified time interval, the contact area does not change in size, but some increments are gained at the beginning of successive time interval. This assumption substantially simplifies the analysis, because it allows one to avoid an algorithmically complex and computationally expensive iterative procedure, for example the one used in [6].

When considering transient deformation of the plate under normal rigid body impact applied to its upper surface, the following non-penetration condition is obtained:

$$u_3^{(\gamma)}(x, y, h, t) - f(x, y) - U(t) = 0\,, \quad \gamma = 1, \ldots, \Gamma \tag{17}$$

Here, $f(x,y)$ is nose shape of the projectile and $u_3^{(\gamma)}(x, y, h, t)$ are normal displacements of the upper surfaces of those bricks (identified by index γ) which are exposed to a contact pressure during given time interval. By applying Lagrange multiplier technique with account for the non-penetration condition, Eqn 17, the following expression is obtained for the interactive energy:

$$V_{IT}(t) = \sum_{\gamma=1}^{\Gamma} \int_{x_l}^{x_{l+1}} \int_{y_m}^{y_{m+1}} \lambda^{(\gamma)}(x, y, t) \left[u_3^{(\gamma)}(x, y, h, t) - f(x, y) - U(t) \right] dxdy \tag{18}$$

Here, $\lambda^{(\gamma)}(x, y, t)$ are the Lagrange multipliers. It should be noted that the above expression explicitly depends on the number of bricks, Γ, interacting with the projectile. Further, the Lagrange multipliers are expanded in double series using the same basis functions as in the primary displacement approximation:

$$\lambda^{(\gamma)}(x, y, t) = \sum_{i=0}^{I} \sum_{j=0}^{J} \Lambda_{ij}^{(\gamma)}(t) X_i(x) Y_j(y) \tag{19}$$

where $\Lambda_{ij}^{(\gamma)}(t)$ are undetermined functions. Substitution of Eqn 19 and Eqn 4 in Eqn 18 yields

$$V_{IP}(t)=\sum_{\gamma=1}^{\Gamma}\sum_{i=0}^{I}\sum_{j=0}^{J}\sum_{p=0}^{I}\sum_{q=0}^{J}\Lambda_{pq}^{(\gamma)}(t)U_{ij}^{(\gamma)}(t)X_{ip}Y_{jq}-\sum_{\gamma=1}^{\Gamma}\sum_{p=0}^{I}\sum_{q=0}^{J}\Lambda_{pq}^{(\gamma)}(t)\left[F_{pq}+U(t)X_pY_q\right] \quad (20)$$

where the following notations were introduced in addition to the earlier notations of Eqn 15:

$$X_p=\int_{x_l}^{x_{l+1}}X_p(x)dx,\ Y_q=\int_{y_m}^{y_{m+1}}Y_q(y)dy,\ F_{pq}=\int_{x_l}^{x_{l+1}}\int_{y_m}^{y_{m+1}}f(x,y)X_p(x)Y_q(y)dxdy \quad (21)$$

Now, all terms in the Lagrange function, Eqn 3, are defined by Eqs 11-13, Eqn 16 and Eqn 20. Total number of unknown functions in this step of analysis contains $3S(I+1)(J+1)(K+1)$ coefficients of the displacement approximation, plus $\Gamma(I+1)(J+1)$ coefficients of the Lagrange multiplier approximations, plus the projectile displacement $U(t)$.

Next step of this algorithmic development includes modification of the Lagrange function, Eqn 3, by incorporating (a) the internal displacement continuity relations, Eqs 8-10, and (b) imposing external kinematic boundary conditions. Then, the Hamilton variational principle is applied to the modified Lagrange function (this procedure can be replaced by directly using the Lagrange equations). Due to a limited space we omit further details of these algorithmic steps. The result is obtained in the form of a linear system of ordinary differential equations, which is then numerically integrated under the respective initial conditions. This routine provides numerical values of the functions $U_{ijk}^{\alpha(s)}(t)$, $\Lambda_{ij}^{(\gamma)}(t)$, and $U(t)$. The transient 3-D fields of displacements, strains and stresses are then obtained by summation of the respective triple series at any given time instant. Summation of the double series, Eqn 19, provides distribution of the contact pressure at the given time instant.

NUMERICAL EXAMPLE

To illustrate capability of the analysis approach described in the previous section, consider numerical example of 3-D impact contact analysis. A bi-material rectangular bar fully clamped at its lower end, $z/c=0$, is exposed to a rigid mass impact at the upper end, $z/c=1$, as shown in Fig. 3. The projectile surface is flat, so $f(x,y)=0$ in this example.

External kinematic boundary conditions and initial conditions are taken as following ($\alpha=1,2,3$):

$$u_\alpha(x,y,z,t)\big|_{z=0}=0 \quad (22)$$

$$u_\alpha(x,y,z,t)\big|_{t=0}=\frac{\partial u_\alpha}{\partial t}(x,y,z,t)\bigg|_{t=0}=0; \qquad U(t)=0,\quad \frac{dU(t)}{dt}\bigg|_{t=0}=V_0 \quad (23)$$

Aluminum bar has the following properties:

$$E_A=73GPa,\quad \nu_A=0.3,\quad \rho_A=2.7\cdot10^3\,kg/m^3 \quad (24)$$

Properties of unidirectional Graphite/Epoxy composite are:

$$E_L=164GPa,\ E_T=9.82GPa,\ G_{LT}=6.78GPa,\ G_{TT}=3.66GPa, \quad (25)$$

$$\nu_{LT}=0.24,\ \nu_{TT}=0.34,\ \rho_C=1.6\cdot10^3kg/m^3$$

Here, reinforcement direction "*L*" coincides with the bar axis *z*. Geometric parameters are:

$$a=b=0.1\ m,\quad c=0.2\ m,\quad c_1=c/3 \quad (26)$$

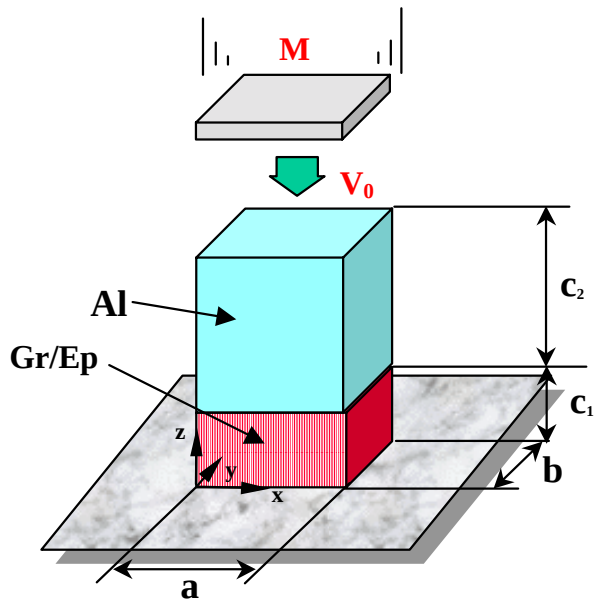

Fig. 3: Longitudinal impact on a bi-material bar

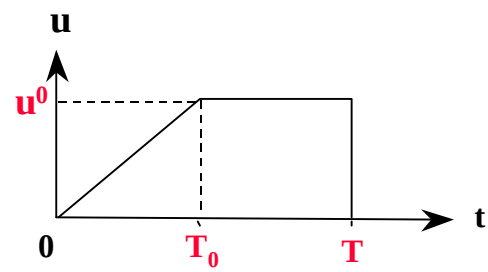

Fig. 4: Assumed shape of the loading history

The normalized time variable $\tau = t / t_0$ is further used, where t_0 is defined as

$$t_0 = c_1 \left(\frac{E_L (1 - \nu_{TT})}{\rho_C (1 - \nu_{TT} - 2\nu_{TL}\nu_{LT})} \right)^{-1/2} + c_2 \left(\frac{E_A (1 - \nu_A)}{\rho_A (1 + \nu_A)(1 - 2\nu_A)} \right)^{-1/2} \tag{27}$$

For the above numerical values used in this example, $t_0 \approx 28\mu \sec$. The projectile mass is taken $M = 90kg$, and its initial velocity $V_0 = 14m/\sec$.

Two distinct 3-D impact analysis approaches are illustrated in the following figures. One of them (further referred as Approach I) corresponds to the contact analysis described in the previous section while the other one (further referred as Approach II) has been presented in [11]. The latter one assumes specific shape of time variation of the longitudinal displacement at the upper end of the bar, as shown in Fig. 4. Two parameters of this loading history, namely, u^0 and T_0, are defined from simple approximate equations following from the energy and momentum conservation laws. However, it is not possible defining the third parameter, the impulse duration *T*. To the contrary, when using the present impact contact analysis, the loading history is not assumed, but obtained directly from the solution, using *M* and V_0 as input parameters.

Variations of the longitudinal displacement and strain are shown in Figs. 5 and 6. Interestingly, the results obtained with both Approaches I and II are very similar for the case of a comparatively low velocity impact under consideration. Particularly, it is seen that the maximum displacement at the loaded end of the bar and slope of the displacement growth during some initial time interval, agree very well with the contact analysis results. At the same time, one advantage of the contact analysis becomes obvious, i.e. this provides also the "declining" branch of the displacement variation, which cannot be defined from the energy and momentum conservation laws.

Another important impact characteristic is contact pressure, which is shown in Fig. 7. Its time variation indicates that the loss of contact between the bar and projectile occurs at $\tau \approx 16$.

Additional results (not shown here) indicate that at the same time instant, the projectile displacement $U(\tau)$ becomes zero, and the projectile velocity $V(\tau)$ changes the sign.

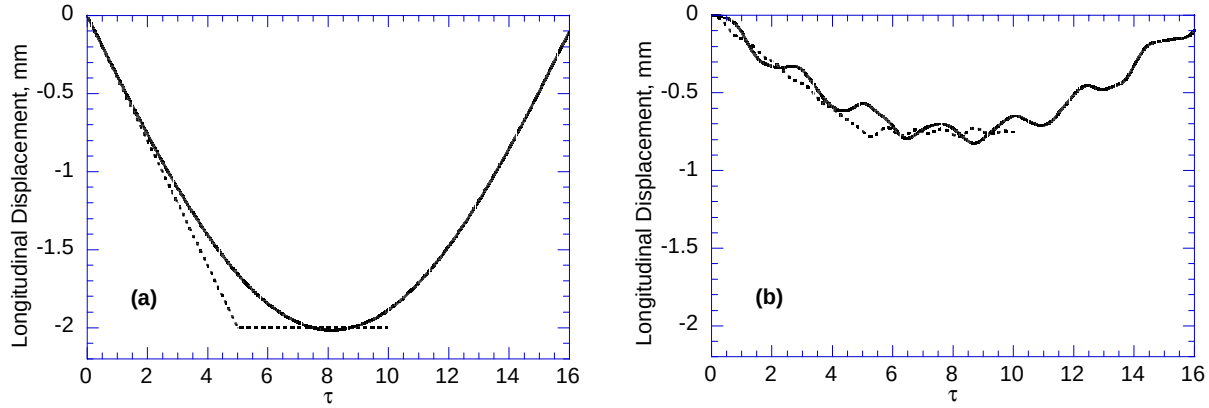

Fig. 5: Variations of the longitudinal displacement u_3 in time at $x/a = y/b = 0.5$ and two values of z: $z/c = 1$ (a) and $z/c = 0.5$ (b). Solid lines correspond to Approach I, dashed lines to Approach II.

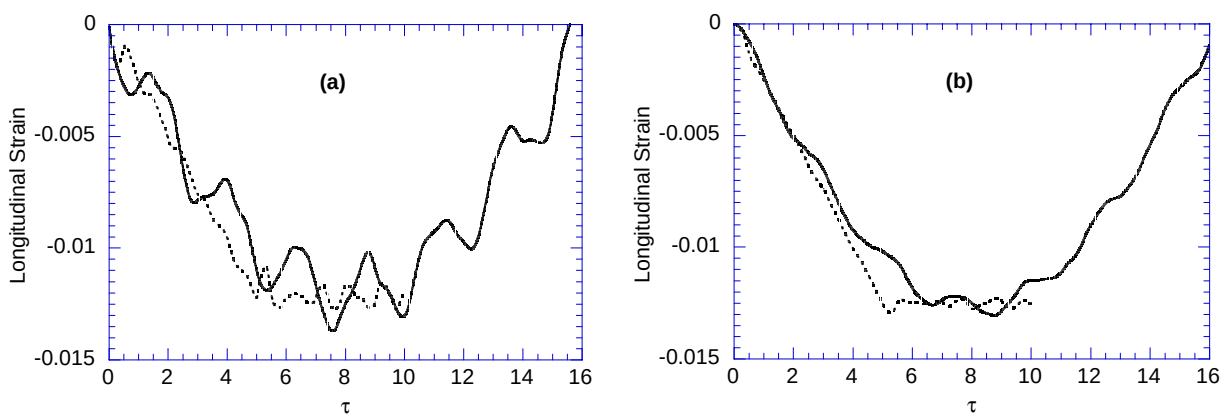

Fig. 6: Variations of the longitudinal strains ε_3 in time at $x/a = y/b = 0.5$ and two values of z: $z/c = 1$ (a) and $z/c = 0.5$ (b). Solid lines correspond to Approach I, dashed to Approach II

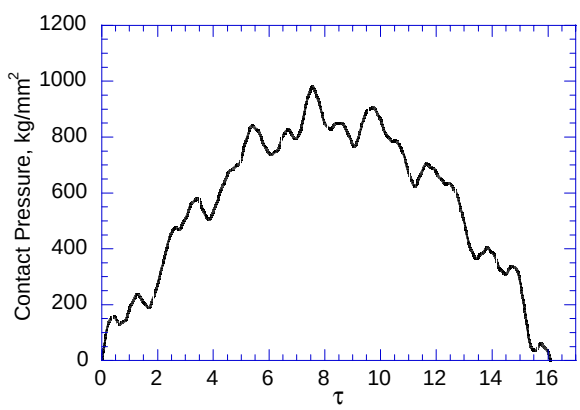

Fig. 7: Time variation of the contact pressure

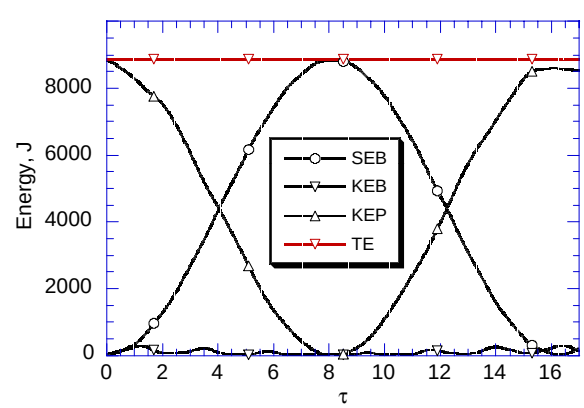

Fig. 8: Time variations of the energy components

In order to illustrate accuracy of the performed variational analysis, we next present in Fig. 8 time variations of the computed strain energy of the bar (SEB), kinetic energy of the bar (KEB), kinetic energy of the projectile (KEP) and total energy of the system (TE). It is seen that the total energy conservation law is accurately satisfied at all time instants during the impact contact process. Besides, at all times the total energy equals to the initial kinetic energy of the projectile. At time instant $\tau \approx 8$ the projectile stops, its velocity and kinetic energy take zero values, the displacement reaches its maximum, and strain energy of the bar also reaches maximum. It is also noticed that kinetic energy of the bar is very small compared to the total energy value. This is easy to explain: mass of the bar is 4.7*kg* while mass of the projectile is 90*kg*.

For the sake of illustrating the effect of projectile mass and velocity, consider now a comparatively "high velocity" and "low mass" impact case: $V_0 = 70\ m/\sec$, $M = 3.3\ kg$. Note that the incipient impact energy is about the same as in the previous, "low velocity" case. Fig. 9 shows that the time variation of the contact pressure is rather different than in the previous case (compare to Fig. 7). The peak magnitude is about the same, though this is reached much sooner (at $\tau \approx 0.2$, as compared to $\tau \approx 8$ in the low velocity case). Further, at $\tau \approx 1.7$ the bar and projectile have almost separated. The contact duration is $\tau \approx 3.3$ while in the low velocity case it was $\tau \approx 16$. These results clearly indicate that it is insufficient to characterize impact phenomenon by the incipient energy only.

Finally, time variations of the energy components for the "high-velocity" case are shown in Fig. 10. The only common feature with the results shown in Fig. 8 is that the total energy remains constant during the entire impact process. However, kinetic energy of the projectile sharply drops to zero at $\tau \approx 2.2$, then it increases, but never gets close to the initial value. Kinetic energy of the bar during initial stage of deformation is about the same as its strain energy, however maximum of the strain energy (reached at $\tau \approx 1.7$) is still significantly higher. It is anticipated that if further increasing initial velocity of the projectile and reducing its mass, the contact duration would further reduce, kinetic energy of the projectile would faster convert into strain energy of the bar and into its kinetic energy (the latter one would gain a higher relative value).

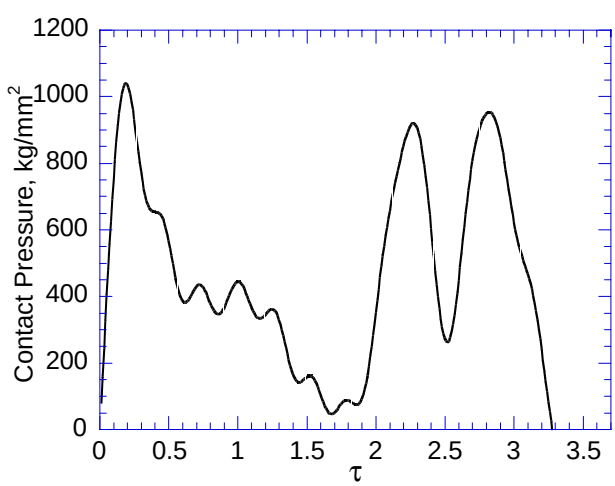

Fig. 9: Time variation of the contact pressure ("high-velocity" impact case)

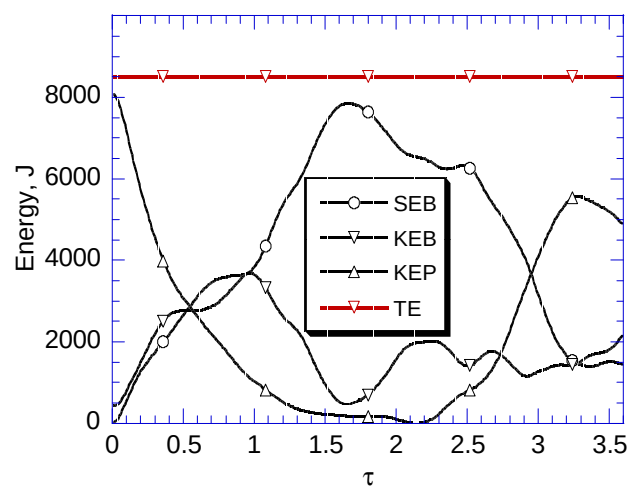

Fig. 10: Time variations of the energy terms ("high-velocity" impact case)

CONCLUSIONS

A novel 3-D variational analysis approach has been developed to solve transient deformation problems of composite structures exposed to a relatively high velocity impact. The approach can be used for laminated, sandwich or textile reinforced composite plates, stiffened panels, bonded joints and other geometries, related to Cartesian coordinate system. The approach is based on the 3-D mosaic body concept; each brick in the body may have its distinct, generally anisotropic elastic properties. The mathematical problem formulation takes in a full consideration 3-D transient nature of impact deformation and, specifically, allows one to study stress wave propagation processes. The adopted impact contact model only considers the mass, initial velocity and nose shape of the projectile as input data; no contact law needs to be assumed. Numerical example of a thick, rectangular bi-material Al-Gr/Ep composite bar, exposed to a longitudinal rigid body impact, has been solved for two combinations of the projectile mass and velocity. The obtained results show that it is inadequate to characterize impact loading in terms of the incipient energy only. The results also show that kinetic energy of the target is of a greater importance at higher impact velocities. Its value may even exceed strain energy of the target if the projectile velocity gets above certain magnitude. Accounting for the energy dissipation and inelastic effects will further enhance capabilities of this variational analysis approach.

REFERENCES

1. Sun, C.T. and Sierakowski, R.L., "Studies on the Dynamic Impact of Jet Engine Blades", *The 43rd Shock and Vibration Bulletin, Pt. 4*, 1973, pp. 11-19.
2. Moon, F.C., "Wave Propagation and Impact in Composite Materials", *Composite Materials Vol. 7*, Chamis C.C., Ed., Academic Press, New York, 1975, pp. 259-332.
3. Takeda, N. and Sierakowski, R.L., "Localized Impact Problems of Composite Laminates", *Shock and Vibration Digest*, Vol. 12, No. 8, 1980, pp. 3-10.
4. Cantwell, W.J. and Morton, J., "The Impact Resistance of Composite Materials - a Review", *Composites*, Vol. 22, No. 5, 1991, pp. 347-362.
5. Abrate, S., “Impact on Laminated Composite Materials”, *Applied Mechanics Reviews*, Vol. 44, No. 4, 1991, pp. 155-190.
6. Bogdanovich, A.E. and Iarve, E.V., “Numerical Analysis of Impact Deformation and Failure in Composite Plates”, *Journal of Composite Materials*, Vol. 26, No. 4, 1992, pp. 520-545.
7. Abrate, S., “Impact on Laminated Composites: Recent Advances”, *Applied Mechanics Reviews*, Vol. 47, No. 11, 1994, pp. 517-544.
8. Sierakowski, R.L. and Chaturvedi, S.K., *Dynamic Loading and Characterization of Fiber-Reinforced Composites*, John Wiley & Sons, New York, 1997.
9. Bogdanovich, A.E. and Yarve, E.V., “Numerical Analysis of Laminated Composite Plates Subjected to Impact Loading”, *Proceedings of the American Society for Composites, Fourth Technical Conference*, Technomic Publ. Co., 1989, pp. 399-409.
10. Bogdanovich, A.E., "Three-Dimensional Variational Theory of Laminated Composite Plates and Its Implementation with Bernstein Basis Functions", to be published in *Computer Methods in Applied Mechanics and Engineering*, 1999.
11. Bogdanovich, A.E. and Yushanov, S.P., "3-D Variational Dynamic Analysis of Laminated Composite Bars and Its Applications", *Extended Abstracts of the Fifth International Conference on Composites Engineering, ICCE/5*, Hui, D., Ed., 1998, pp.97-98.
12. Davis, P.J., *Interpolation & Approximation*, Dover Publications, New York, 1975.